AIChE

Analysis of Mixing in a Twin Cam Mixer Using Smoothed Particle Hydrodynamics

Martin Robinson
School of Mathematical Sciences, Monash University, Clayton, Victoria 3169, Australia

Paul Cleary
CSIRO Mathematical and Information Sciences, Clayton, Victoria 3169, Australia

Joseph Monaghan
School of Mathematical Sciences, Monash University, Clayton, Victoria 3169, Australia

DOI 10.1002/aic.11530
Published online June 13, 2008 in Wiley InterScience (www.interscience.wiley.com).

Smoothed Particle Hydrodynamics (SPH) is a Lagrangian, particle-based method that is well suited to industrial mixing simulations. Mass transport is simply the motion of the particles, and its grid-free nature means that it can easily accommodate complicated geometries involving moving parts and sharp corners. This article describes 2D SPH simulations of a Twin Cam mixer and compares the results against experimental data and results from two published finite element method (FEM) simulations. To analyze the mixing processes in the Twin Cam mixer, we present a method for calculating the Finite-Time Lyapunov Exponent (FTLE) using SPH particle data. The FTLEs can be used to locate the unstable and stable manifolds in the flow and indicate where mixing is either promoted or inhibited in the flow. We also present a local measure of how two or more fluids are "mixed" at a point in the domain. This is used to find the time-scales of mixing over different regions in the domain and at different length-scales. The purpose of the article is to evaluate the effectiveness of SPH, FTLEs, and our mixing measure in simulating and analyzing the mixing in a typical industrial mixer. © 2008 American Institute of Chemical Engineers
AIChE J, 54: 1987–1998, 2008
Keywords: smoothed particle hydrodynamics, mixing, Lyapunov Exponents, Twin Cam mixer, chaotic transport

Introduction

Smoothed particle hydrodynamics

Numerical simulations of fluid flow in typical industrial mixers are difficult because of complicated geometries involving moving parts and sharp corners. Grid-based methods such as Finite Element Methods (FEM) need to constantly regenerate the mesh to accommodate the moving objects, and these meshes often need to be further refined to correct the model fluid flow near small gaps and sharp corners. Smoothed Particle Hydrodynamics (SPH) is a Lagrangian, particle-based method that does not suffer from these disadvantages. Instead of a grid it makes use of particles, which are both interpolation points for the fluid variables as well as physical volumes of fluid. Boundaries are constructed

Correspondence concerning this article should be addressed to M. Robinson at martin.robinson.monash.edu.au.

from similar particles, which can be moved at each timestep or arranged to form sharp corners with insignificant computational overhead.

Because of its Lagrangian nature SPH is well-suited to modeling mixing problems, which require solving the advection of two or more interacting fluids. Each particle represents a volume of fluid, so advection is obtained from the motion of the particles. Two or more fluids with different physical properties are also simple to model, as each fluid is represented by its own set of particles.

See Monaghan[1] for a good review of SPH theory.

Twin Cam mixer experiments and simulations

The experimental validation in this article uses data from the work of Avalosse and Crochet.[2] They used a Twin Cam mixer to track the mixing of a colored volume of fluid using a very low Reynolds Number (Re = 0.001). Without the action of turbulent diffusion at these low Reynolds numbers, knowledge of the mixing processes and the mixer design becomes very important in providing uniform and efficient mixing. Applications in this regime include food and polymer processing. Avalosse and Crochet compared their experimental results of the Twin Cam mixer with a 2D finite-element method (FEM) simulation. Their base mesh was a regular grid in circular coordinates, with a constant angular resolution, and with the radial resolution higher near the circle formed by the rotating tips of the triangular cams. The elements that intersected the straight edges of the cams were re-meshed at every timestep using an automatic algorithm based on Delaunay triangulation. Bertand et al.[3] modeled a similar 2D Twin Cam simulation using FEM. However, instead of using a standard FE method that requires re-meshing at every timestep, they used the Lagrange multiplier-based fictitious domain method. This was combined with an adaptive mesh refinement at each timestep, which was applied around the Cam tips.

Measuring mixing

Ottino[4] has developed a popular mixing theory, which is based on the calculation of several variables along the paths of material points in the flow. He has proposed a commonly used measure of mixing strength: length stretch χ. Avalosse and Crochet[2] applied this measure to their simulation of the Twin Cam mixer. If dx is a material length that deforms into dX after time T, then Ottino's length stretch is defined as

$$\chi(dX,t) = \lim_{|dx|\to 0} \frac{|dX|}{|dx|} \tag{1}$$

Ottino's length stretch is directly related to the chaos theory notion of Lyapunov Exponents σ, which are a measure of how quickly material trajectories diverges from their initial conditions and an indication of chaos if $\sigma > 0$. The Lyapunov Exponent is calculated from Ottino's length stretch by taking its limit over an infinite time period

$$\sigma = \lim_{T\to\infty} \frac{1}{T} \ln \chi \tag{2}$$

Usually the Lyapunov Exponent of interest is the maximum over all possible orientations of the initial material length. All further references in this article refer to the maximum Lyapunov Exponent. As with length stretch, higher values of σ can indicate a higher strength of mixing locally at that point, because a patch of material in an area of high σ will be stretched out, exposing more surface area to the surrounding material. The Lyapunov Exponent has the advantage over Ottino's length stretch in that it does not depend on the initial orientation of the material length and only depends on the maximum stretching, which is the quantity of interest for incompressible mixing. Lyapunov Exponents can also be used to find the stable and unstable manifolds of the flow, which provide information about the global mixing processes. These manifolds are explained in more detail in the next section. Although Lyapunov Exponents are only useful for periodic flows, as the flow must be fully defined over infinite time, the concept has been extended to finite times (Finite Time Lyapunov Exponents, FTLE) and finite sizes (FSLE).[5–8]

As well as a measure of the quality of mixing at a point, there is also a need to calculate how "mixed" two or more materials are. There are many different methods to calculate this, many depending on the particular application. Poux[9] describes nearly 50 different mixing measures proposed in the literature. However, all of these measures are global. They can be used to calculate the amount of mixing locally by dividing up the region of interest. However, as most of the methods are based on statistical analysis, there must be sufficient sample points in each region to reduce the error to a reasonable level. We present a mixing measure that easily calculates the amount of mixing locally, with fewer sample points needed.

Chaotic transport

One of the important features of a chaotic system are its stable and unstable invariant manifolds and their associated hyperbolic or stagnation points. Knowledge of the location and movement of these features gives important insight into the mixing and transport of the system.[4,10,11]

The process of mixing can be described in terms of the stretching and folding of the flow. The fluid is stretched apart along the stable manifolds and folded along the length of the unstable manifolds. Figure 1 shows this process diagrammatically.

A stable manifold has the defining property that a material point, initialized on a stable manifold, will approach its hyperbolic point as $t\to\infty$. The labeling of these manifolds as "stable" is often confusing, as the definition of stability for these manifolds differs from the traditional engineering view. Using the traditional view of stability, one might expect that a point initialized on or near a stable manifold would approach that manifold over time and be resistant to small perturbations. However, the opposite is true. Any perturbation to a material point on a stable manifold will cause the particle to move further away from that manifold. The labeling of this type of manifold as stable actually refers to the stable nature of the hyperbolic point within the 1D domain of the manifold itself. Material points initialized within this domain approach the hyperbolic point over time, and are resistant to tangential perturbations along the manifold.

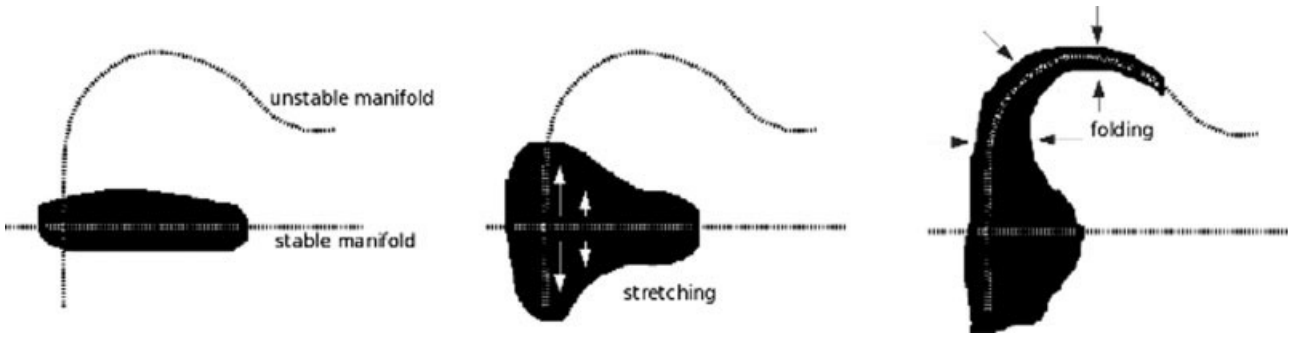

Figure 1. Diagram showing how an initial blob of fluid is first stretched out away from the stable manifold and then folded along the length of the unstable manifold.

The property of stable manifolds most related to the mixing is that a pair of particles straddling the manifold will separate faster than any other nearby pairs (except of course for a pair across the same manifold). It is this last property that can be exploited to find the manifolds. FTLEs are a (finite-time) measure of the exponential divergence of two closely spaced points, so the maxima in the spatial distribution of FTLE indicate the presence of a stable manifold. However, it must be noted that this is not always the case. Regions of maximum shear will also show up as FTLE maxima, hence care must be taken when interpreting the results.

A similar description, but reversed in time, can be used for unstable manifolds. A material point initialized on an unstable manifold will approach its hyperbolic point in reverse time ($t \to -\infty$). Additionally, a pair of particles straddling the unstable manifold will separate faster than any other nearby pairs in reverse time (i.e. they will approach the manifold faster than any other nearby pairs). Hence, calculating the FTLE spatial distribution using a negative time step T will once again show the unstable manifolds as maxima in the FTLE distribution. Note again that the labeling of these manifolds as "unstable" is quite different from the traditional view of stability and refers only to the nature of the hyperbolic point within the 1D domain of the manifold. A material point initialized near an unstable manifold will approach the manifold over time and be resistant to small perturbations.

The Simulation Method

All the equations in this section, along with additional explanation, can be found the 2005 review paper by Monaghan.[1] The most commonly used kernel for SPH simulations (and the kernel used in this simulation) is the cubic spline. In two dimensions, this has the form:

$$W(r,h) = \frac{1}{h^2}\frac{15}{14\pi}\begin{cases} (2-q)^3 - 4(1-q)^3, & \text{for } 0 \le q \le 1 \\ (2-q)^3, & \text{for } 1 < q \le 2 \\ 0, & \text{for } q > 2 \end{cases} \tag{3}$$

where $q = r/h$ and h is the smoothing length of the particle. The kernel determines how the mass of particle is spread out in space, as well as how the fluid variables are interpolated between particles.

The SPH version of the momentum equation for particle a is:

$$\frac{d\mathbf{v}_a}{dt} = -\sum_b m_b \left(\frac{P_b}{\rho_b^2} + \frac{P_a}{\rho_a^2} + \Pi_{ab}\right)\nabla_a W_{ab} + \sum_k m_k(\mathbf{f}_{ak} - \Pi_{ak}\nabla_a W_{ak}) \tag{4}$$

where $\prod_{ab}$ is a viscosity term between particles a and b and $\mathbf{f}_{ak}$ is the force between boundary particle k and particle a. The first sum is over all the SPH particles within $2h$ of particle a, whereas the second sum is over all the boundary particles within the same area. P_a is the pressure, ρ_a is the density and m_a is the mass of particle a. There are a number of forms for the viscosity term. We are using the form:

$$\begin{aligned} \Pi_{ab} &= -\frac{\alpha v_{\text{sig}}(\mathbf{v}_{ab}\cdot\mathbf{r}_{ab})}{\overline{\rho}_{ab}|\mathbf{r}_{ab}|} \\ v_{\text{sig}} &= c_a + c_b - \beta \mathbf{v}_{ab}\cdot\hat{\mathbf{r}}_{ab} \\ \mathbf{v}_{ab} &= \mathbf{v}_a - \mathbf{v}_b \\ \mathbf{r}_{ab} &= \mathbf{r}_a - \mathbf{r}_b \\ \overline{\rho}_{ab} &= \frac{1}{2}(\rho_a + \rho_b) \end{aligned} \tag{5}$$

where $\beta \approx 4$ and α is related to the dynamic viscosity μ by:

$$\alpha = \frac{114\mu}{15\rho c_s h} \tag{6}$$

where c_s is the sound speed. The standard form of the continuity equation for constant h is:

$$\frac{d\rho_a}{dt} = \sum_b m_b \mathbf{v}_{ab}\cdot\nabla_a W_{ab} \tag{7}$$

The equation of state models a nearly incompressible fluid, and is given by:

$$P_a = B\left(\left(\frac{\rho_a}{\rho_0}\right)^{\gamma} - 1\right) \tag{8}$$

where $\gamma = 7$ and ρ_0 is a reference density. The pressure scale factor B is given by:

$$B = \frac{100\, v_{\max}^2 \rho_0}{\gamma} \tag{9}$$

where $v_{\max}$ is an estimate of the maximum flow velocity.

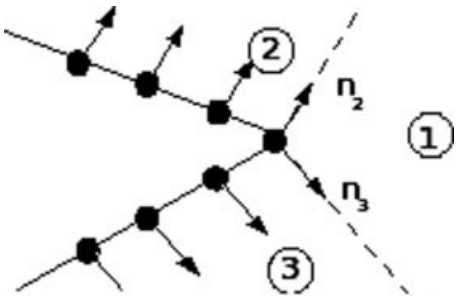

Figure 2. Multiple boundary normals for sharp corners.

For a fluid particle in Region 2, use n_2. In Region 3 use n_3. In Region 1 use unit radial vector in the direction from the corner particle to the fluid particle.

The tank walls and triangular cams are modeled using boundary particles, which are fixed to the boundary and exert boundary and viscous forces on the other SPH particles (i.e. the rightmost sum in Eq. 4). The boundary force per unit mass on particle a from a boundary particle k, where x is the tangential distance (i.e. along the boundary) between k and a and y is the normal distance between k and a, is given by

$$\mathbf{f}_{ak} = -\frac{m_a}{m_a + m_k} B(x, y)\mathbf{n}_k \tag{10}$$

where $\boldsymbol{n}_k$ is the unit normal vector to the boundary. B is chosen so that it increases rapidly for small y (so as to prevent the particle from penetrating the wall) and so its variation with x ensures that the particle feels no change in force as it moves tangentially along the boundary, see Monaghan[1] for the form of B used here.

Finding the correct normal vector $\boldsymbol{n}_k$ can be difficult near sharp corners in the boundary. Large changes in the direction of neighbouring boundary normals can lead a very small value of y (since $y = |\boldsymbol{n}_k \cdot \boldsymbol{r}_{ab}|$), which results in an unnaturally large boundary force. To fix this problem, each sharp point is represented with a particle that has two normals equal to those of its neighboring boundary particles. The correct $\boldsymbol{n}_k$ is calculated from these normals and the position of the interacting fluid particle (see Figure 2 and Monaghan[12]).

Mixing Analysis

Finite-time Lyapunov Exponent

The Finite-Time Lyapunov Exponent (FTLE) is calculated considering the trajectories of particles over a finite-time period T. What follows is a brief derivation of the FTLE, see the excellent description by Shadden[13] for a more in-depth discussion. Consider two material points in the flow at $t = t_0$, separated by $\delta\mathbf{x}$. Gradients in the velocity field between the two points will cause their separation to change over time. Using a first order approximation of the velocity gradient, the separation after time T, $\delta\mathbf{X}$, will be (using tensor component notation)

$$\delta X^i = \left(\frac{\partial v^i}{\partial x^j}\,\delta x^j\right) T \tag{11}$$

The magnitude of this separation is given by

$$\|\delta\mathbf{X}\| = T\sqrt{\delta x^i \,\frac{\partial v^j}{\partial x^i}\,\frac{\partial v^j}{\partial x^k}\,\delta x^k} \tag{12}$$

The maximum separation of the two particles will occur when they are aligned along the eigenvector associated with the largest eigenvalue of $\partial\mathbf{v}/\partial\mathbf{x}$. Thus, if $\lambda_{\max}$ is the absolute value of the maximum eigenvalue of $\partial\mathbf{v}/\partial\mathbf{x}$, then

$$\max\left\|\delta\mathbf{X}\right\| = \lambda_{\max}\left\|\overline{\delta\mathbf{x}}\right\| T \tag{13}$$

where the bar over $\delta\mathbf{x}$ indicates that it is aligned with the eigenvector corresponding to $\lambda_{\max}$. This can be written

$$\max\|\delta\mathbf{X}\| = e^{\sigma T}\|\overline{\delta\mathbf{x}}\| \tag{14}$$

where σ is the FTLE. That is, the magnitude of the exponential separation velocity between two neighboring particles. Re-arranging to obtain an expression for σ

$$\sigma = \frac{1}{T}\ln(\lambda_{\max} T) \tag{15}$$

Grid-based numerical methods use tracer particles to calculate the FTLE. Because the tracers can be initialized on a regular grid, finite-differencing can be used to estimate the spatial velocity gradient $\partial\mathbf{v}/\partial\mathbf{x}$. In an SPH simulation, the SPH particles are used and they will typically not be regularly spaced. However, the gradient can be found at a particular SPH particle a by using a linear least-squares method on the irregularly spaced particles surrounding the base particle. Assume a linear velocity gradient around particle a given by

$$\begin{aligned} v^i(x^j) &= A^{ij}(x^j - x_a^j) + v_a^i \\ A^{ij} &= \frac{\partial v_i}{\partial x_j} \end{aligned} \tag{16}$$

Consider a particle b with an initial separation from a of $\delta\mathbf{x}_{ab}$. After time T the SPH simulation will have calculated the final separation $\delta\mathbf{X}_{ab}$ of these particles. Using the linear velocity gradient, the final separation $\delta\mathbf{X}_{ab}$, is related to the initial separation $\delta\mathbf{x}_{ab}$ by

$$\delta X_{ab}^i = A^{ij}\delta x_{ab}^j T \tag{17}$$

In principle, only two such particles would be needed to solve Eq. 17 for the velocity gradient components A^{ij}. However, since the velocity gradient is very sensitive to errors in the particle separations, we have chosen to use all of the particles within the smoothing length ($2h$) of the base particle a (i.e. the base particle's neighbors). It is reasonable to assume that the velocity gradient will be constant over this area. Using these N particles, A^{ij} is found by minimizing the sum

$$\sum_b^N (\delta X_b^i - A^{ij}\delta x_b^j T)^2 \tag{18}$$

Once the velocity gradient is found, its maximum eigenvalue can be found and substituted into Eq. 15 to find the FTLE of particle a. This entire process can then be repeated for all the SPH particles within the domain.

Mixing measure

This section describes a measure M that indicates how "mixed" two or more sets of SPH particles are, given a particular length scale. At larger length scales equal to the entire domain, all the particles by definition are completely mixed ($M = 1$). At length scales equal to the distance between the particles, the particles are completely segregated ($M = 0$). This is a local measure of the mixing, so a spatial distribution of the mixing can be generated using this measure.

Consider a SPH particle a and all the particles within a distance r_m. Each particle a has a color c_a. The basis for the mixing measure is that the particles are defined to be totally mixed if the color ratios present in the subregion are the same as the global ratios. Given this, we propose a mixing measure equal to the dot product of these two ratios. That is,

$$M = \mathbf{s}_\mathrm{l} \cdot \mathbf{s}_\mathrm{g} \tag{19}$$

where $\boldsymbol{s}_\mathrm{l}$ is a vector of the ratios of different colored particles in the subregion, scaled by the total number of particles of each color. The ratio vectors are both in a color number space of dimension C, where C is the number of different colors present. Therefore, $\boldsymbol{s}_\mathrm{l}$ is given by

$$\mathbf{s}_l = \frac{1}{\sqrt{\sum_{i=1}^{C}\left(\frac{n_i}{N_i}\right)^2}}\left(\frac{n_1}{N_1}, \frac{n_2}{N_2}, \ldots, \frac{n_C}{N_C}\right) \tag{20}$$

where n_i is the number of particles in the local subregion with $c_a = i$ and N_i is the total number of particles in the simulation with $c_a = i$. The global ratio $\boldsymbol{s}_\mathrm{g}$ is simply $\boldsymbol{s}_\mathrm{l}$, which is evaluated over the entire flow region. That is:

$$\mathbf{s}_\mathrm{g} = \frac{1}{\sqrt{C}}(1, 1, \ldots, 1) \tag{21}$$

The mixing measure is then normalized between 0 (no mixing) and 1 (totally mixed). Therefore

$$\begin{aligned} M &= \frac{\mathbf{s}_\mathrm{l} \cdot \mathbf{s}_\mathrm{g} - M_\mathrm{min}}{1 - M_\mathrm{min}} \\ M_\mathrm{min} &= \frac{1}{\sqrt{C}} \end{aligned} \tag{22}$$

where the minimum value of $M = M_\mathrm{min}$ occurs when all the particles in the subregion are of a single color.

This measure is invariant to translation and rotation of the spatial coordinate system. It changes linearly with the color ratios in the subregion and does not depend on the initial coloring of the particles, since $\mathbf{s}_\mathrm{g}$ is invariant.

Simulation Results

Experimental validation

A diagram of the Twin Cam geometry is shown in Figure 3. The fluid used for the experimental results was a Newtonian aqueous solution of glucose, with a viscosity of 50 Pa s and a density of 1500 kg/m^3. The counter-clockwise rotating cams are moving at 0.5 rpm, which gives a Reynolds number of the order of 0.001.

The results of the SPH simulation can be validated against the experiment performed by Avalosse and Crochet.[2] Figure 4 shows the initial conditions for both the SPH simulation and experiment (top row). This figure also shows the simulation and experiment after the cams have rotated through 1 revolution (middle row) and 1 1/3; revolutions (bottom row), taken at times 120 and 160 s, respectively.

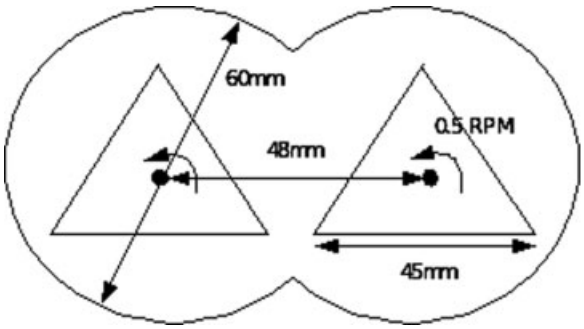

Figure 3. Geometry of Twin Cam mixer.

The motion of the cams divides the colored blob into two segments along a line that is roughly diagonal from the lower right tip of the left cam to the top of the right cam (This line is actually a stable manifold of the flow. See Figure 7, top, for an image of this line). There is a stationary point at the center of the domain, so particles near this point have a lower velocity. This causes a trail of particles behind the bulk of the colored particles as they leave the centre of the domain, which shortens to form a "kink" or "hook" in the blob (seen most clearly in the lower region of the leftmost chamber at $t = 120$ s). The blob is stretched out as it is moved around the chamber, because of lower velocities near the walls of the chamber. Once the leading edges of the divided blobs have completed a revolution, and are once again between the cams, both are further divided along the same line as the initial division, and the mixing process continues.

The transport of the colored blob of fluid follows the experiment well. Over a period of 1 Cam revolution (middle row), most of the features of the colored blob are captured by the simulation. The main deviations from the experiment occur at the leading edge of the two colored segments formed when the initial blob is torn apart. Once these two segments return to the centre of the mixer, the highly chaotic central region amplifies any transport errors accumulated during the simulation. At 4/3 cam revolutions (bottom row), the general features of the colored blob can be seen in the simulation, but some are reasonably different from the experiment (for example, the upper T feature in the experiment near the center of the domain is not reproduced in the simulation).

Adding more particles can reduce the numerical errors present in the SPH simulation. However, it was found that increasing the number of particles did not correctly model either the upper T feature (shown at 4/3 Cam revolutions) or the leading wedge in the left cam (shown at 1 Cam revolution just above the lower right corner of the left Cam). These two features were also not modeled correctly in the Finite Element simulations of Avalosse and Crochet and Bertrand et al., indicating that there is a physical process that is not being modelled in any of the simulations (e.g. 3D effects).

Figure 5 compares the SPH simulation against the two Finite-Element simulations by Avalosse and Crochet[2] and

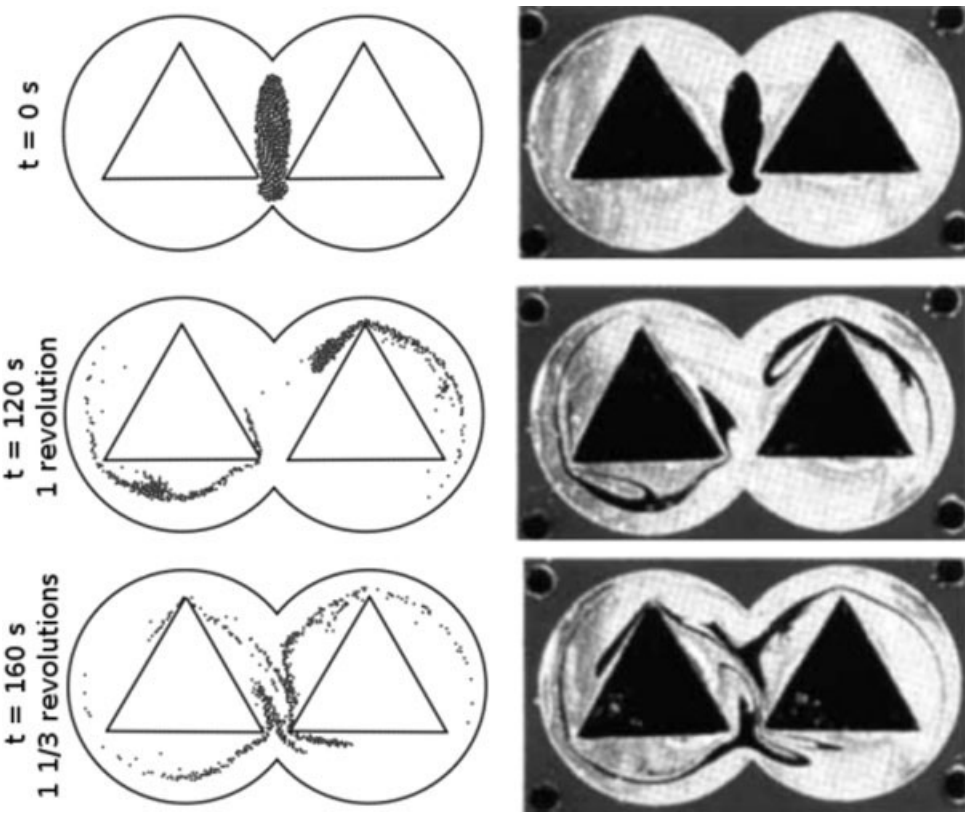

Figure 4. Comparison between the experiment performed by Avalosse and Crochet[2] (right), and the SPH simulation results (left).

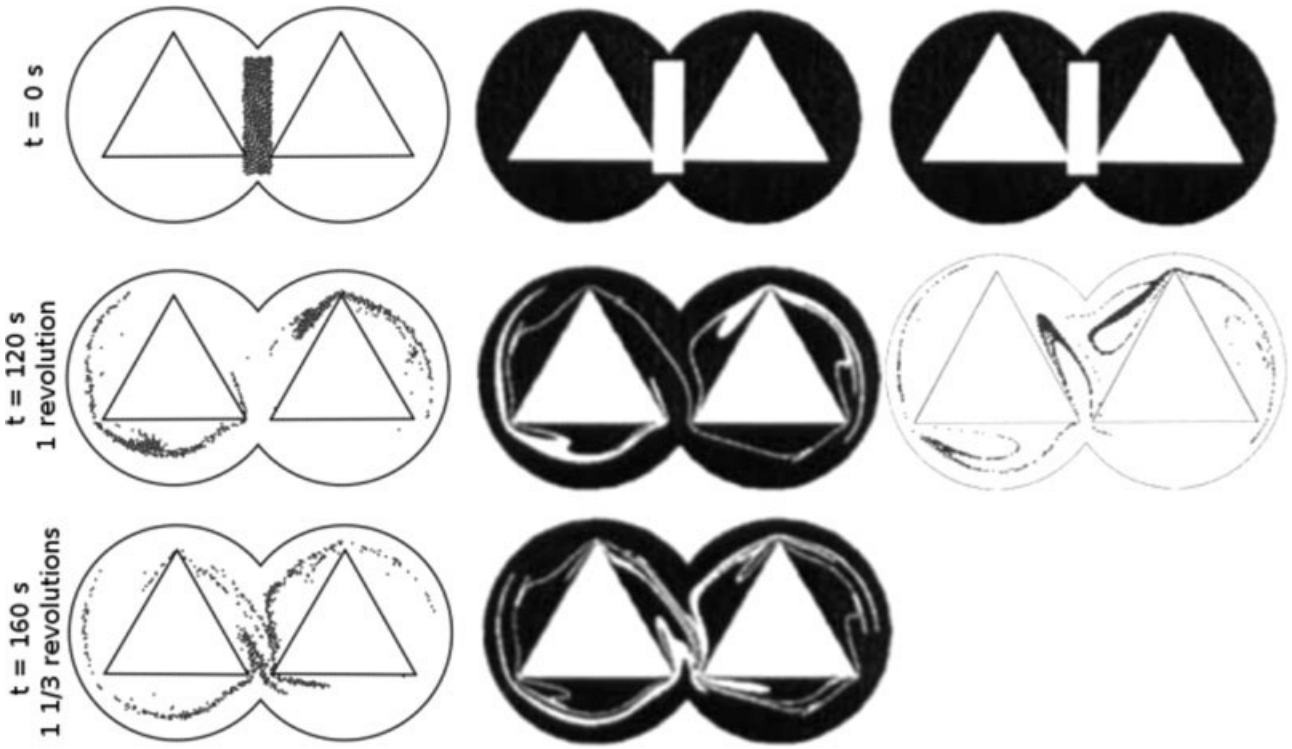

Figure 5. Comparison of SPH simulation (left column), the simulation by Avalosse and Crochet[2] (middle column) and the simulation by Bertand et al.[3] (right column) at three different times.

The top row shows the initial distribution of the colored blob, the middle row shows the blob at $t = 120$ s (i.e. after 1 Cam revolution) and the bottom row shows the blob at $t = 160$ s (4/3 Cam revolutions).

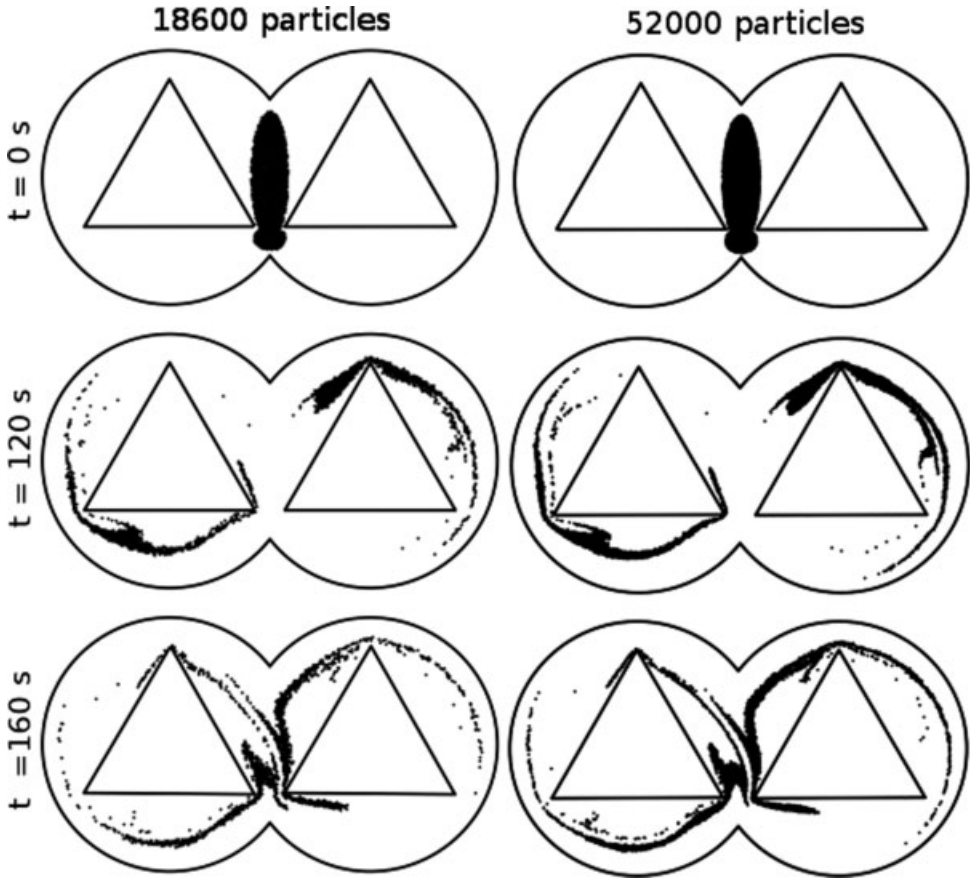

Figure 6. SPH simulation using an increased resolution of 18,600 and 52,000 particles.

Bertand et al.[3] The initial conditions of both FEM simulations are only a rectangular approximation to the experimental blob, so we have initialized the SPH simulation using a similar rectangular blob. All the simulations have problems capturing the leading edge of the two separated segments. Avalosse and Crochet's simulation and the SPH simulations both underestimate the size of these two features, whereas Bertrand's overestimates them. The features of the blob in the SPH simulation are remarkably similar to Avalosse and Crochet's, except that the SPH simulation does not have the erroneous striations coming out from the centre of the domain. Overall, the SPH simulation, with no adaptive resolution or remeshing requirements, compares very well with both the FEM simulations.

The SPH simulations shown in Figures 4 and 5 use 7995 particles (160 particles along the horizontal). Avalosse and Crochet use 7724 grid points in their simulation. Bertrand et al. initially uses 2388 finite elements to represent the domain, but this is before the mesh refinement around the cam edges. Using a rough visual estimate, the total number of elements after the mesh refinement was ~6000. Hence, all three simulations have roughly comparable resolution. At this resolution, running the SPH simulations takes about 22 min per cam revolution on a single 3.2GHz Pentium 4 processor.

Timestep and viscosity issues

The viscous time scale can be estimated from that of a flow between two concentric cylinders (Batchelor,[14] p. 203). Taking the distance between the cylinders as $d = 10$ mm and assuming the inner cylinder is rotating with the same period as the cams while the outer is at rest, we find:

$$\frac{t_{\text{visc}}}{t_{\text{cam}}} = \frac{\rho d^2/\pi^2\mu}{120} \approx 2.5 \times 10^{-6} \tag{23}$$

Since SPH is an explicit method, with a viscous timestep:

$$\delta t_{\text{visc}} \approx \frac{\rho h^2}{\mu} = 3 \times 10^{-5} \tag{24}$$

the SPH simulation would need 4×10^6 steps to allow the cams to move through one revolution. This is impractical for what should be a small-scale 2D simulation.

However, since the time-scale of the viscous forces is so small compared with the rotating cams, the viscosity can be significantly reduced without affecting the transport of the fluid. The ratio $t_{\text{visc}}/t_{\text{cam}}$ will increase but remain much less than 1. This will increase the time needed for the viscous forces to equilibrate to a state that balances the pressure and boundary forces, but as long as this timescale remains very small compared with the rotational timescale this will not affect the flow dynamics or the transport of the fluid.

The viscosity in these simulations was therefore reduced to 0.005 Pa s in order to speedup the explicit integration. This is a factor of 10^{-4} smaller than the experimental viscosity and $t_{\text{visc}}/t_{\text{cam}} \sim 2.5 \times 10^{-2}$. The simulation has been run with higher viscosities up to 0.05 Pa s, demonstrating no dis-

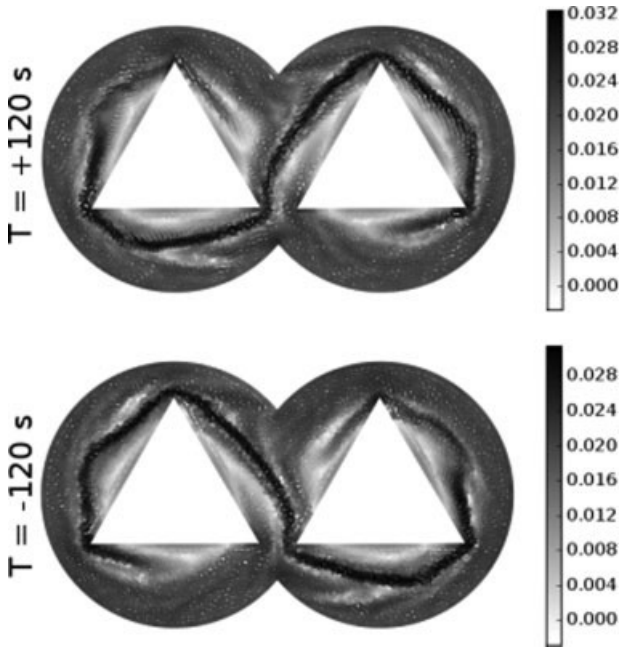

Figure 7. Top: Forward-time FTLE with $T = +1$ cam revolution and $t = 0$ s.

Bottom: Reverse-time FTLE with $T = -1$ cam revolution.

tinguishable effect on the results, which confirms that the reduced viscosity has negligible impact on the solution.

Increased resolution

To establish that the results had converged and no more improvement could be gained from additional resolution, the SPH simulation was run again with an increased resolution of 18,600 particles (240 particles across the horizontal) and 52,000 particles (400 across the horizontal). The results are presented in Figure 6. There is no change in the general shape of the colored blob over the first cam revolution, indicating that the results have converged over this timescale. However, after the first 120 s the chaotic flow tends to amplify small changes. In particular, the slight sharpening of the "hook" just below the left cam at $t = 120$ s leads to a change in the blob shape near the lower right corner of the left cam at $t = 160$ s.

A significant advantage of the higher resolution is that the particles more smoothly represent the blob's shape and pick up finer detail. To achieve this result without increasing the resolution, massless particles could be added to the simulation. These would not change the movement of the SPH particles, but would cheaply "fill in" the details of the blob of interest.

Mixing Results

Finite-time Lyapunov Exponents

Figure 7 shows the results of calculating both the forward and backward time Finite-Time Lyapunov Exponent (FTLE) over a time interval of 1 cam rotation. The maxima ridges in these plots (indicated by the dark coloration) clearly show the location of the main stable and unstable manifolds. These manifolds are redrawn together in Figure 8, along with the results at two subsequent times. This figure shows both the location of the manifold's fixed hyperbolic point (the intersection of the stable and unstable manifolds at the center of the domain) as well as the many homoclinic points formed as the two manifolds crisscross each other around the cams. A homoclinic point is the intersection of a stable and an unstable manifold originating from the same hyperbolic point. As $t \to \infty$, these points will approach that hyperbolic point. The presence of transverse homoclinic points (which these points are) indicates the presence of chaotic orbits, which are essential for good mixing.

The location of the manifolds in Figure 8 shows the geometry of the stretching and folding actions of the mixer. The blob of fluid surrounding the cams is stretched out along the stable manifold and folded around the cams along the unstable manifold. However, the particular geometry of these manifolds means that not all of their effects on the mixing

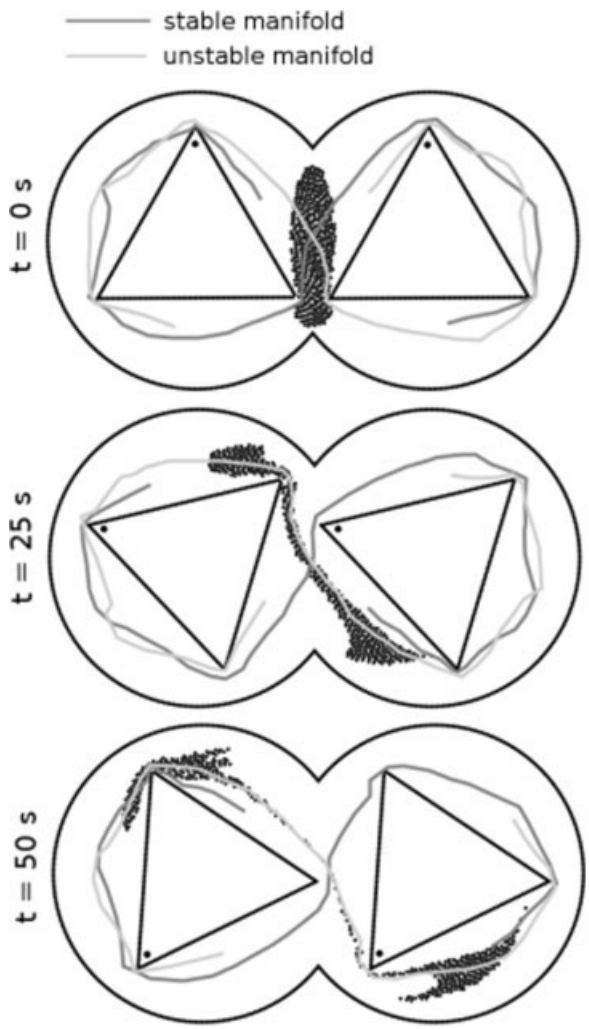

Figure 8. Top: The unstable and stable manifolds shown in Figure 7, redrawn together along with the colored blob of fluid.

Middle and bottom: Similar plots of the manifolds at subsequent times.

are positive. Both stable and unstable manifolds act as separatrices for the flow, i.e. there is very little flux of material across these lines. For the Twin Cam mixer, this means that fluid is trapped between the tangle of manifolds and the cams and does not mix with the rest of the domain. With respect to the mixing measure M introduced earlier, this means that the slowest increase of M overtime would be obtained by initially coloring the particles between the manifold and the Cams a different color from the rest of the domain. This is explored in more detail further on in this article (see Figure 12).

Counter-rotating simulation

The previous simulations had the two Cams rotating in the same direction at a constant speed of 0.5 rpm. This configuration is expected to produce good mixing. For the case where the cams are rotating at the same speed but opposite directions, the experiment performed by Avalosse and Crochet[2] indicates that there should be little or no mixing between the two chambers of the mixer. This provides an interesting case to explore what happens to the manifolds in a poor mixing case, as well as a simple test of the simulation accuracy. Figure 9 shows the results for this case.

The top plot in Figure 9 shows the particles initialized at $t = 0$ (middle plot) so that the particles in the left chamber are of different color to the right. The plot below this shows the particles at $t = 245$ s. The interface between the two different colors is preserved almost exactly, even though the fluid particles have been rotated though just over two periods. The small flux of particles from one chamber to the other near the top corner of the outside chamber $(x,y) = (60,55)$ (in mm) is a physical effect. The experiment by Avalosse and Crochet[2] showed a similar flux.

The bottom two plots shows the SPH particles colored according to their forwards and backwards-time FTLE (calculated using $T = \pm 120$ s). This shows a linear vertically orientated, strong unstable and stable manifold at $x = 60$ mm. Because both manifolds are coincident, every point along their length is a homoclinic point. However, these are degenerate homoclinic points, which, unlike the transverse kind, do not indicate chaotic mixing. Furthermore, these manifolds act as separatrices, and this prevents any fluid in the left chamber from entering the right and vice versa.

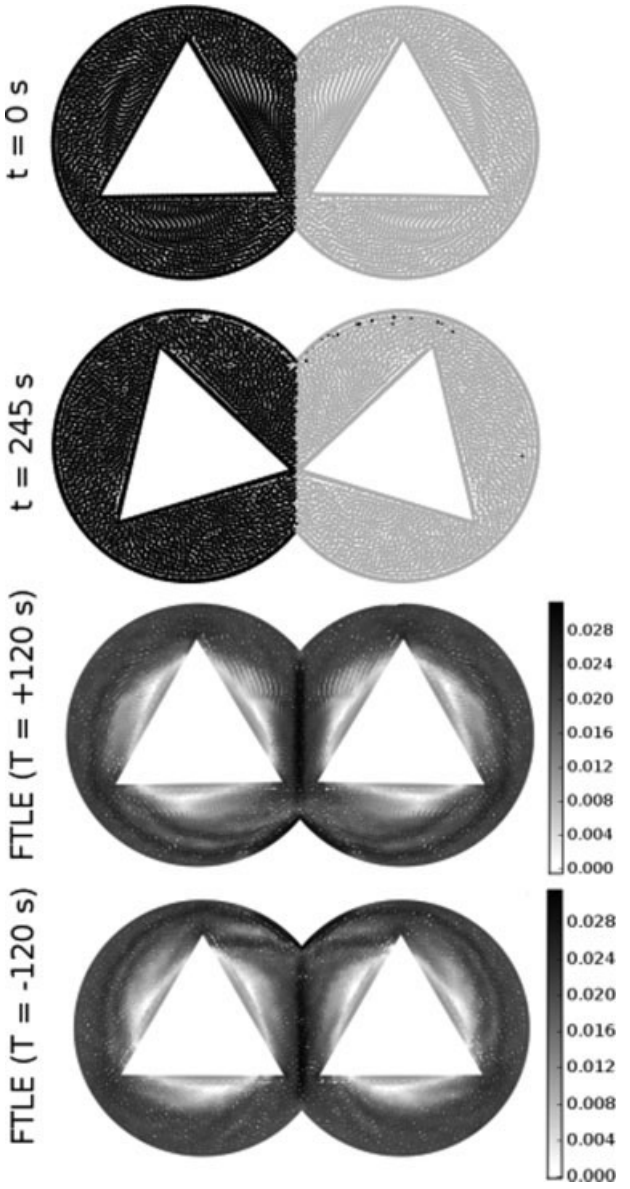

Figure 9. Counter-rotating twin cam simulation.

Top, Colored particles at $t = 0$ s; Middle top, coloured particles at $t = 245$ s; Middle bottom, FTLE with $T = +120$ s; Bottom, FTLE with $T = -120$ s.

Mixing measure and timescales

This section explores the timescales of the mixing, and in particular the effect that the tangle of manifolds has on these timescales. Figure 10 shows the same Twin Cam mixer simulation with particles once again colored so that the domain is split evenly between two colors. Once again the two cams are rotating in the same direction (counter-clockwise) at a constant speed of 0.5 rpm. The location of the mixed particles is shown after 500 s (just over four cam rotations), as is a plot of the particles colored by the amount of mixing using the mixing measure M defined previously and a length scale (i.e. radius of the subregions used to calculate the mixing measure) of $r_m = 3.25$ mm.

Mixing between the two chambers proceeds rapidly. After 500 s the light and dark particles are significantly mixed in the outer regions of the mixer. However, the inner regions are largely unmixed and are still primarily composed of their original particles. This is expected, since we have already determined from the FTLE maps that the tangle of manifolds wrapped around the cams prevents fluid in this inner region from mixing with the rest of the domain, because of the manifolds acting as separatricies.

Compare this with the simulation depicted in Figure 11, where the particles are colored so that the inner regions between the manifolds and the Cam walls are colored grey (this region is approximated as a circular area). For these initial conditions, the only mixing possible is between the inner and outer regions, and as can be seen, over the 500 s the only mixing that occurs is a slow diffusion of the colors near the boundary. This confirms the analysis based on the separatrices from the FTLE calculations.

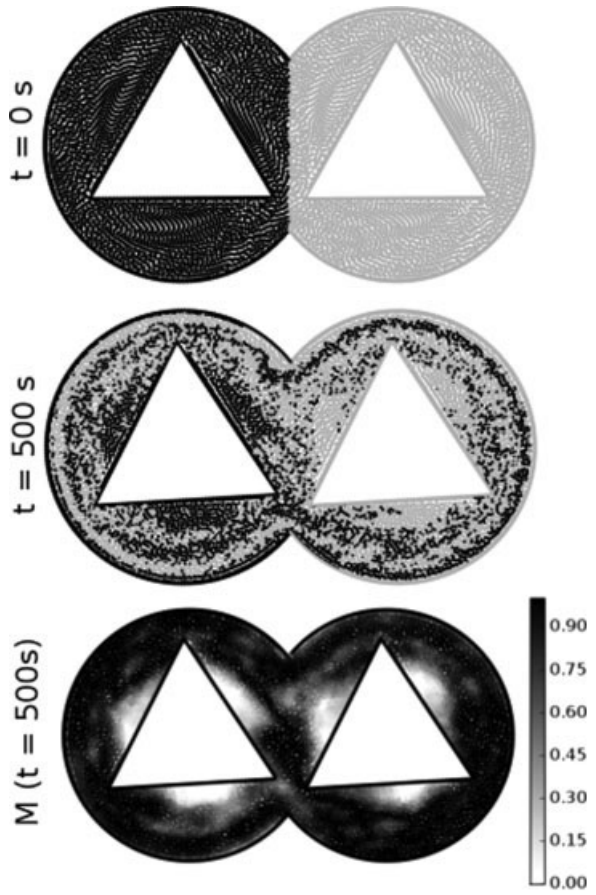

Figure 10. Particles in each mixing chamber colored separately.

The two cams are both rotating counter-clockwise at 0.5 rpm (the original configuration). Top, Colored particles at $t = 0$ s; Middle, colored particles at $t = 500$ s.

To get a clear idea of the timescales of mixing for these two different initial particle colorings, Figure 12 plots the mean mixing measure M (taken over the entire domain) vs. time for both cases. Changing the radius of the subregions used to calculate the amount of mixing shows how the fluid is mixed over different length scales. The smallest subregion radius used is 0.8125 mm, which is 1/150th of the width of the domain or just over the average distance between each particle (the distance between the particles are ~120/160 mm). The largest radius used is 15 mm, which is 1/8th of the domain width.

The left column in Figure 12 shows the first case, where the particles in each chamber of the mixer are given different colors. Because the fluid transport in this case is dominated by mixing outside the tangle of manifolds, this gives an indication of the mixing time-scales in the outer region. As can be seen, all of the length scales plotted reaches a plateau close to their maximums by around 1000 s (8.3 revolutions). Before this time, it can be seen that the slope of M increases for larger length scales. This means that larger length scales are mixing more quickly than the smaller, which is an indication of the greater effect of the chaotic mixing process compared with the smaller scale diffusion processes.

An interesting anomaly in the mixing plot on the left side is the periodic mixing and unmixing for the larger length scales during the first 1500 s. The cause of this anomaly is not fully understood, but is probably caused by the length scales being too large to properly resolve the interface between the two colors.

The right plot in Figure 12 shows the second case, where particles inside the tangle of manifolds are given a different color to the rest of the domain. These particles start out more mixed than the first case, because of the larger interface between the two colors, especially at larger length scales. However, the rate of mixing is significantly reduced in this case. Even after 5000 s the mean mixing measure still has not reached a maximum. The rate of mixing for different length scales is also very different than the previous case. The slope of M now increases for smaller length scales, indicating that diffusion processes, rather than chaotic mixing, play a larger role in the mixing.

Conclusion

SPH is very well suited to modeling mixing processes. There is no need to numerically solve any extra equations in

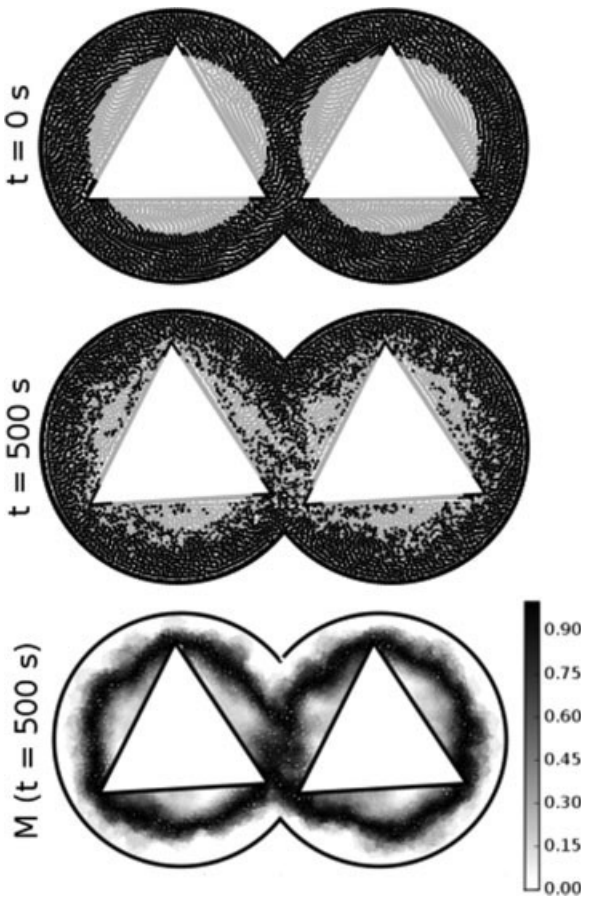

Figure 11. Particles colored gray between the tangle of manifolds and the Cam walls.

The two cams are both rotating counter-clockwise at 0.5 rpm. Top, colored particles at $t = 0$ s; Middle, colored particles at $t = 500$ s; Bottom, mixing measure M at $t = 500$ s and using $r_m = 3.25$ mm.

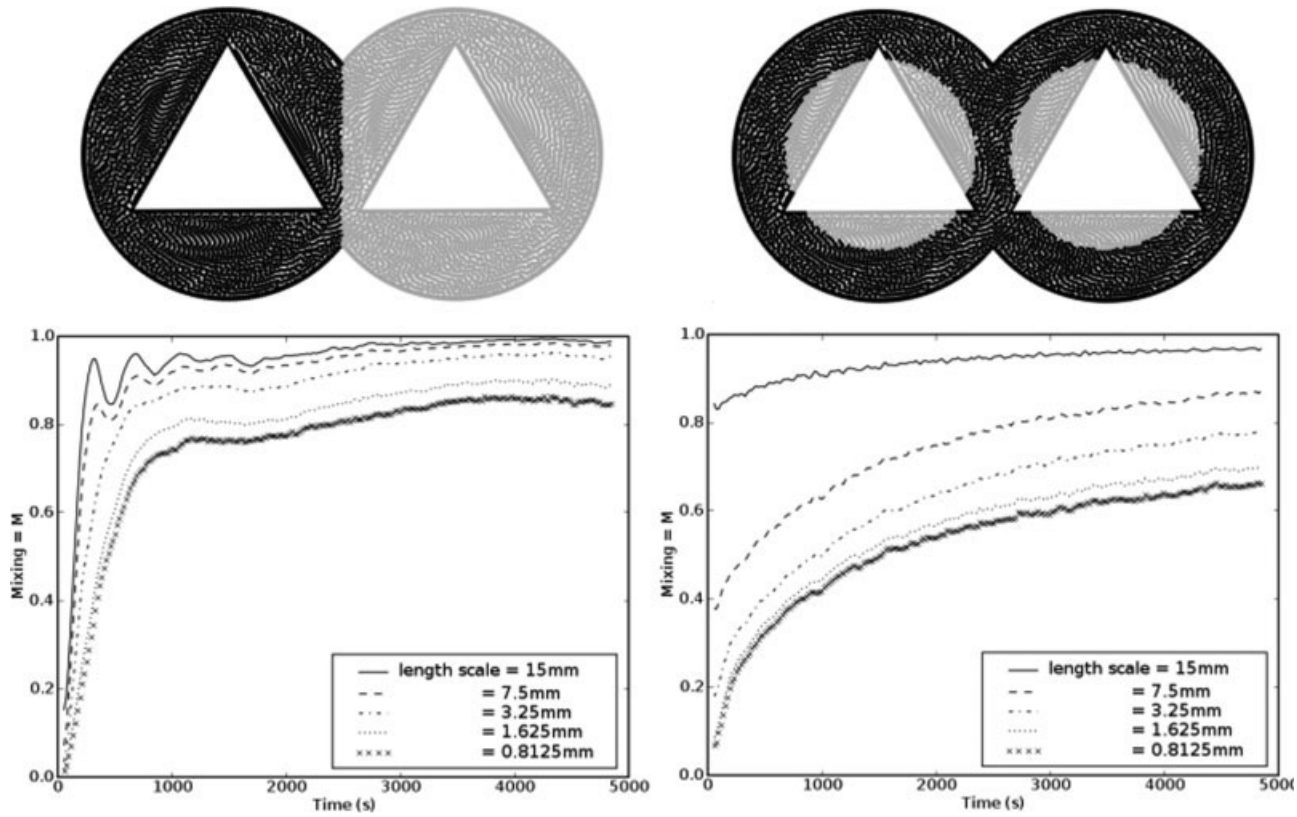

Figure 12. Mean *M* (taken over the entire domain) vs. time for the initial conditions depicted in the top row of figures.

The left side shows the mixing between the two chambers over time, whereas the right shows the mixing between the inner region trapped by the tangle of manifolds and the rest of the domain. Each line plot represents a different length scale used to calculate the mixing. $M = 0$ indicates no mixing whereas $M = 1$ indicates that the fluids are fully mixed. A full revolution of the cams takes 120 s, so the mixing plots show about 41 revolutions. Both cams are rotating counter-clockwise.

order to track material points or determine concentrations, as each particle represents a volume of fluid for the duration of the simulation. Moving objects with sharp corners, essential to any practical mixer, are also simply modeled via moving boundary particles. Most importantly, the fluid transport is accurately modeled. The SPH simulation of a Twin Cam mixer compares well against experiment and two other finite-element simulations.

FTLE spatial maps are useful tools for analyzing chaotic mixing. They can be used to locate stable and unstable manifolds in the flow, which provides valuable information on the barriers for mixing to a given piece of mixing equipment and where mixing is best promoted. We have presented a method of obtaining FTLE spatial maps directly from SPH particle data, and analyzed the mixing processes in the Twin Cam mixer. When corotating, this mixer generates chaotic orbits in the outer portion of the domain, which promotes mixing in this region. However, the tangle of stable and unstable manifolds surrounding the cams act as separatrices in the flow and prevent fluid transport out of a region close in to the flat edges of the cams, so this area does not mix well with the fluid in the rest of the domain. When the mixer is counter-rotating, the stable and unstable manifolds are coincident in a single, linear line down the centre of the domain, preventing fluid transport from one chamber to the other. Because the manifolds have no transverse intersection points, no chaotic orbits are generated and there is no significant mixing of the fluid.

We have also developed a local measure of the amount of mixing at any point in the domain. This can be used to generate a spatial map of the amount of mixing at various length scales. As well as giving information on the time-scales of mixing over different areas of the domain, this measure can also be used to explore the time-scales of mixing at larger or shorter length-scales, which gives an indication of the relative effects of chaotic mixing (which, for the Twin Cam mixer, will operate most strongly at the length-scale of the cams) and diffusion processes (which have the most effect at shorter length scales).

Literature Cited

1. Monaghan JJ. Smoothed particle hydrodynamics. *Rep Prog Phys*. 2005;68:1703–1759.
2. Avalosse T, Crochet MJ. Finite-element simulations of mixing: 1. Two-dimensional flow in periodic geometry. *AlChE J*. 1997;43:577–587.
3. Bertand F, Thibault F, Delamare L, Tanguy PA. Adaptive finite element simulation of fluid flow in twin-screw extruders. *Comput Chem Eng*. 2003;27:491–500.
4. Ottino, JM. *The Kinematics of Mixing: Stretching, Chaos and Transport*. Cambridge: Cambridge University Press, 1989.

5. Artale V, Boffetta G, Cellani A, Cencini M, Vulpiani A. Dispersion of passive tracers in closed basins: beyond the diffusion coefficient. *Phys Fluids*. 1997;9:3162–3171.
6. Pierrehumbert RT, Yang, H. Global chaotic mixing on isentropic surfaces. *J Atmos Sci*. 1993;50:2462–2480.
7. Lapeyre G. Characterization of finite-time Lyapunov exponents and vectors in two-dimensional turbulence. *Chaos*. 2002;12:688–698.
8. Joseph B, Legras B. Relation between kinematic boundaries, stirring, and barriers for the Antarctic polar vortex. *J Atmos Sci*. 2002;59: 1198–1212.
9. Poux M, Fayolle P, Bertand J, Bridoux D, Bousquet J. Powder mixing: some practical rules applied to agitated systems. *Powder Technol*. 1991;68:213–234.
10. Holmes P. Poincare, celestial mechanics, dynamical-systems theory and Chaos. *Phys Rep*. 1990;193:137–163.
11. Rom-Kedar V, Leonard A, Wiggins, S. An analytical study of transport, mixing and chaos in an unsteady vortical flow. *J Fluid Mech*. 1990;214:347–394.
12. Monaghan JJ, Kos A, Issa N. Fluid motion generated by impact. *J Waterway Port Coastal Ocean Eng*. 2003;129:250–259.
13. Shadden, S. Lagrangian coherent structures: analysis of time-dependent dynamical systems using finite-time Lyapunov exponents. Available at http://www.cds.caltech.edu/~shawn/LCS-tutorial/. 2005. Last accessed June 2008.
14. Batchelor GK. *An Introduction to Fluid Dynamics*. Cambridge: Cambridge University Press, 1967.

Manuscript received Sept. 16, 2007, revision received Feb. 27, 2008, and final revision received Apr. 24, 2008.